Oxidation of Carbon Monoxide on Group 11 Metal Atoms: Matrix-Isolation Infrared Spectroscopic and Density Functional Theory Study

Qiang Xu* and Ling Jiang

National Institute of Advanced Industrial Science and Technology (AIST), Ikeda, Osaka 563-8577, Japan, and Graduate School of Science and Technology, Kobe University, Nada Ku, Kobe, Hyogo 657-8501, Japan

Received: September 12, 2005; In Final Form: December 14, 2005

Laser-ablated Cu, Ag, and Au atoms react with CO and O_2 mixture in solid argon to produce carbonyl metal oxides, $(O_2)Cu(CO)_n$ ($n = 1, 2$), (η^1-OO)MCO (M = Ag, Au), $OCAuO_2CO$, and OAuCO, as well as group 11 metal carbonyls and oxides. These carbonyl metal oxides are characterized using infrared spectroscopy on the basis of the results of the isotopic substitution and the CO concentration change. Density functional theory (DFT) calculations have been performed on these molecules. The identifications of these carbonyl metal oxides are confirmed by the good agreement between the experimental and calculated vibrational frequencies, relative absorption intensities, and isotopic shifts. Carbon dioxide is eliminated from these carbonyl metal oxides upon UV irradiation, providing the evidence for the oxidation of carbon monoxide on group 11 metal atoms. The present experiments also reveal that the reactivity of copper toward CO is prior to O_2, and the reactivity of silver toward O_2 is prior to CO, whereas the reactivity of gold toward CO is comparable to O_2.

Introduction

The oxidation of carbon monoxide is of considerable interest from an academic and an industrial viewpoint due to its importance in many practical applications such as combustion exhaust, the development of CO detection devices, and improved efficiency of CO_2 lasers.[1] Extensive research efforts have been made both experimentally and theoretically to search for suitable catalysts to enhance this oxidation process.[1−7] It has been found that gold becomes catalytically active when deposited on select metal oxides as hemispherical ultrafine particles with diameters smaller than 5 nm.[1,2] The supported Au nanoparticles exhibit remarkable catalytic activities and/or excellent selectivities in a number of reactions such as low-temperature CO oxidation and the reduction of nitrogen oxides.[1,2] The reactivity of gold cluster and/or anions toward CO and O_2 has received much attention in the recent past.[1−7] The investigations of the combustion of CO on supported, size-selected gold clusters Au_n ($n \leq 20$) have shown that the CO oxidation is size-dependent in nature with Au_8 being the smallest cluster to catalyze the reaction.[3] Mass-spectrometry-based studies of the coadsorption of CO and O_2 on small gold clusters have revealed that CO and O_2 adsorb cooperatively rather than competitively.[5,6] Furthermore, Au_6^- has been identified to be highly active for the CO + O_2 reaction.[5] Interestingly, a combined photoelectron spectroscopic and theoretical investigation of $Au_6(CO)_n^-$ ($n = 0−3$) has indicated that an electron shuttling from the outer triangle to the inner triangle takes place upon CO chemisorption in the negatively charged systems and that the neutral $Au_6(CO)_n$ complexes should be reactive toward O_2 due to the destabilization of the highest occupied molecular orbital of Au_6 upon CO chemisorption.[7] On the other hand, the so-called "low-temperature" Cu/ZnO catalyst is widely used to catalyze the water gas shift (WGS) reaction ($CO + H_2O \rightarrow CO_2 + H_2$) and metallic Cu provides the active site for catalysis.[8] In the surface redox mechanism, CO reacts with adsorbed oxygen atom to produce CO_2.[8] Recent experimental and theoretical investigations reveal that the WGS reaction can be promoted by preadsorbed oxygen by its acting either as a promoter or as a reaction intermediate.[9]

Recent studies have shown that, with the aid of isotopic substitution, matrix-isolation infrared spectroscopy combined with quantum chemical calculations is very powerful in investigating the spectrum, structure, and bonding of novel species and the related reaction mechanisms.[10,11] In contrast to the extensive experimental and theoretical studies of the oxidation of carbon monoxide to carbon dioxide by gold clusters or nanoparticles, however, to the best of our knowledge little attention has been paid to systematic investigation of the oxidation of carbon monoxide on group 11 metal atoms. Here we report a study of the reactions of laser-ablated Cu, Ag, and Au atoms with CO/O_2 mixtures in argon matrixes. IR spectroscopy coupled with theoretical calculations provides evidence for the oxidation of carbon monoxide to carbon dioxide on group 11 metal atoms.

Experimental and Theoretical Methods

The experiment for laser ablation and matrix-isolation infrared spectroscopy is similar to those previously reported.[12] Briefly, the Nd:YAG laser fundamental (1064 nm, 10 Hz repetition rate with 10 ns pulse width) was focused on the rotating Cu, Ag, and Au targets. The laser-ablated metal atoms were co-deposited with CO/O_2 mixtures in excess argon onto a CsI window cooled normally to 7 K by means of a closed-cycle helium refrigerator. Typically, 1−15 mJ/pulse laser power was used. The CO (99.95%), $^{13}C^{16}O$ (99%, $^{18}O < 1\%$), $^{12}C^{18}O$ (99%), O_2 (99.5%), $^{18}O_2$ (99% ^{18}O), scrambled O_2 ($^{16}O_2/^{16}O^{18}O/^{18}O_2 = 1:2:1$), and mixed isotopic samples were used to prepare the CO/Ar mixtures. In general, matrix samples were deposited for 1−2 h with a typical rate of 2−4 mmol/h. After sample deposition, IR spectra were recorded on a Bio-Rad FTS-6000e spectrometer at 0.5 cm^{-1} resolution using a liquid nitrogen cooled HgCdTe (MCT) detector for the spectral range of 5000−400 cm^{-1}. Samples were annealed at different temperatures and subjected

* To whom correspondence should be addressed. E-mail: q.xu@aist.go.jp.

10.1021/jp055155d CCC: $33.50
Published on Web 02/04/2006

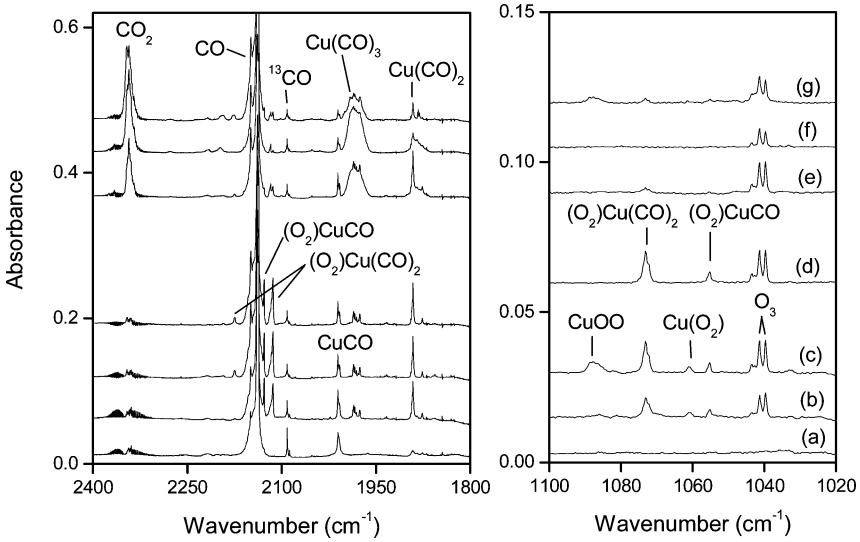

Figure 1. Infrared spectra in the 2400−1800 and 1100−1020 cm^{-1} regions from co-deposition of laser-ablated Cu atoms with 0.5% CO + 0.25% O_2 in Ar: (a) 1 h of sample deposition at 7 K; (b) after annealing to 25 K; (c) after annealing to 30 K; (d) after 20 min of $\lambda > 600$ nm irradiation; (e) after 20 min of $\lambda > 340$ nm irradiation; (f) after 20 min of broad-band irradiation; (g) after annealing to 34 K.

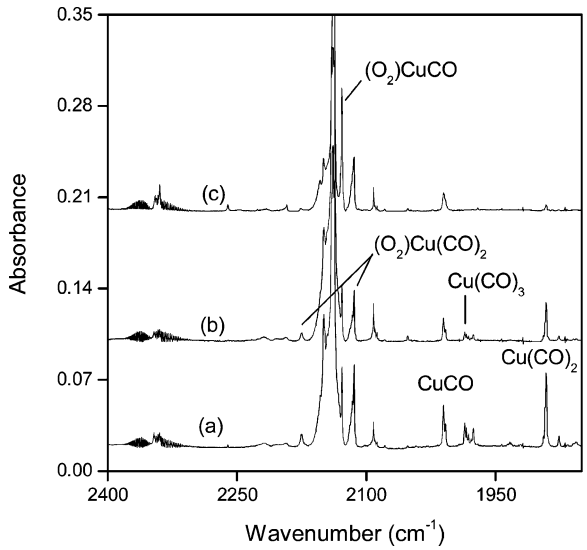

Figure 2. Infrared spectra in the 2400−1800 cm^{-1} region for laser-ablated Cu atoms co-deposited with different CO and O_2 concentrations in Ar after annealing to 30 K: (a) 0.5% CO + 0.25% O_2; (b) 0.5% CO + 0.5% O_2; (c) 0.5% CO + 5.0% O_2.

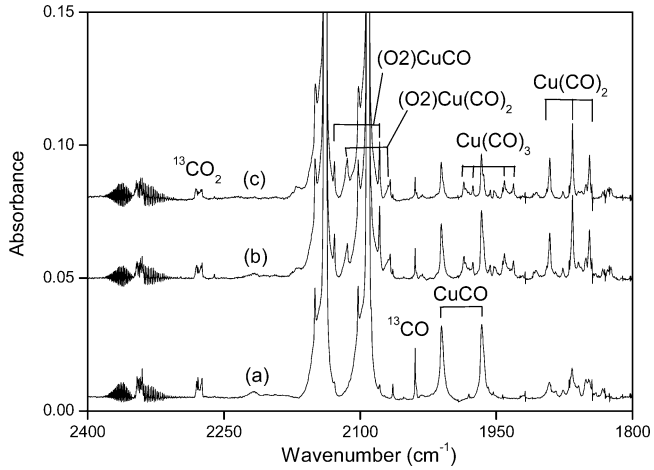

Figure 3. Infrared spectra in the 2400−1800 cm^{-1} region from co-deposition of laser-ablated Cu atoms with 0.35% $^{12}C^{16}O$ + 0.35% $^{13}C^{16}O$ + 0.25% O_2 in Ar: (a) 1 h of sample deposition at 7 K; (b) after annealing to 25 K; (c) after annealing to 30 K.

to UV−vis irradiation ($\lambda > 250$ nm) using a high-pressure mercury arc lamp (Ushio, 100 W), and more spectra were recorded.

Quantum chemical calculations were performed to predict the structures and vibrational frequencies of the observed reaction products using the Gaussian 03 program.[13] The B3LYP density functional method was used.[14] The 6-311+G(d) basis set was used for C and O atoms,[15] and the Los Alamos ECP plus DZ (LANL2DZ) was used for Cu, Ag, and Au atoms.[16] Geometries were fully optimized and vibrational frequencies were calculated with analytical second derivatives. Additional BP86 and BLYP[14] calculations gave similar results and will not be reported here.

Results and Discussion

Experiments have been done with CO and O_2 concentrations ranging from 0.05% to 5.0% in excess argon. Typical infrared spectra for the reactions of laser-ablated Cu, Ag, and Au atoms with CO/O_2 mixtures in excess argon in the selected regions are illustrated in Figures 1−9, and the absorption bands in different isotopic experiments are listed in Table 1. Absorptions common to these experiments such as metal carbonyls, metal oxides, O_3, O_4^-, O_4^+, and O_6^+ have been reported previously[17−20] and are not listed here. The stepwise annealing and photolysis behavior of the product absorptions is also shown in the figures and will be discussed below. Experiments have also been done with doping CCl_4 of different concentrations serving as an electron scavenger in solid argon. It has been found that doping with CCl_4 has no effect on these bands, suggesting that the products are neutral.[21] Meanwhile, experiments have also been done for the co-deposition of laser-ablated group 11 metal atoms with separate CO and O_2 samples to confirm the new absorptions.

Quantum chemical calculations have been carried out for the possible isomers and electronic states of the potential product molecules. Figure 10 shows the most stable structures of the reaction products. The ground electronic states, point groups, vibrational frequencies, and intensities are listed in Table 2. Table 3 reports a comparison of the observed and calculated isotopic frequency ratios for the C−O and O−O stretching modes of the reaction products.

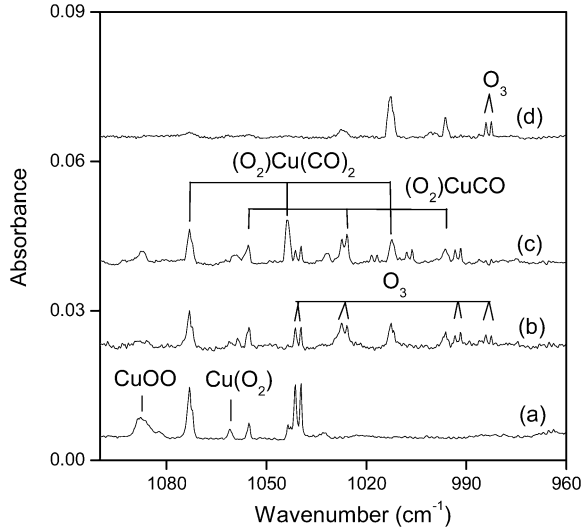

Figure 4. Infrared spectra in the 1100−960 cm^{-1} region from co-deposition of laser-ablated Cu atoms with isotopic CO/O_2 mixtures in Ar after annealing to 30 K: (a) 0.5% CO + 0.25% O_2; (b) 0.5% CO + 0.2% $^{16}O_2$ + 0.2% $^{18}O_2$; (c) 0.5% CO + 0.2% $^{16}O_2$ + 0.4% $^{16}O^{18}O$ + 0.2% $^{18}O_2$; (d) 0.5% CO + 0.25% $^{18}O_2$.

Cu + CO + O_2. New bands at 2128.3 and 1055.3 cm^{-1} (Table 1 and Figure 1) appeared together upon sample annealing. They almost did not change after $\lambda > 600$ nm photolysis, but sharply decreased on $\lambda > 340$ nm photolysis, disappeared after broad-band irradiation, and did not recover upon further annealing. For the 2128.3 cm^{-1} band, the mixed $^{12}C^{16}O$ + $^{13}C^{16}O$ + O_2 isotopic spectra (Figure 3) only provide the sum of pure isotopic bands, indicating that only one CO subunit is involved in this mode. The lower mode (1055.3 cm^{-1}) shifted to 996.2 cm^{-1} with $^{18}O_2$ and gave the $^{16}O/^{18}O$ isotopic ratio of 1.0593. The scrambled CO + $^{16}O_2$ + $^{16}O^{18}O$ + $^{18}O_2$ sample (Figure 4, trace c) presented the oxygen isotopic triplet pattern with 1:2:1 intensity profile at 1055.3, 1025.9, and 996.2 cm^{-1}, showing the intermediate isotopic component very near the average of the pure isotopic bands, which suggests that two equivalent oxygen atoms are involved in this vibration. Furthermore, no intermediate isotopic band was observed in the CO + $^{16}O_2$ + $^{18}O_2$ experiment (Figure 4, trace b). Accordingly, the absorptions at 2128.3 and 1055.3 cm^{-1} are assigned to the C−O and O−O stretching modes of $(O_2)CuCO$, respectively.

The bands at 2174.7, 2114.2, and 1073.1 cm^{-1} have been observed together after sample annealing. As shown in Figure 2, the experimental condition with lower CO/O_2 ratio favors the formation of $(O_2)CuCO$ with the 2128.3 cm^{-1} band (trace c), whereas that of higher CO/O_2 ratio (trace a) favors the formation of the species with the 2114.2 cm^{-1} band, suggesting that the species with the 2114.2 cm^{-1} band carries more CO ligand than the $(O_2)CuCO$ species (2128.3 cm^{-1}). The mixed isotopic pattern (Figures 3 and 4) show that the absorptions at 2174.7, 2114.2, and 1073.1 cm^{-1} can be assigned to the symmetric C−O, asymmetric C−O, and O−O stretching vibrations of $(O_2)Cu(CO)_2$, respectively. It is noted that the reaction of Cu with CO/O_2 mixture is quite different from the case of Cu reaction with CO_2 in solid matrixes, which gave the neutral $CuCO_2$ complex[22a] and the insertion molecular anion $OCuCO^-$ and addition anion $CuCO_2^-$.[22b]

The density functional theory (DFT) calculations lend strong support for the assignments. $(O_2)CuCO$ is predicted to have a C_{2v} symmetry (Figure 10) with a $^2A_2$ ground state (Table 2), which lies 58.32 kcal/mol lower than the quartet one. The calculated C−O and O−O stretching frequencies of the (O_2)-CuCO species are 2190.3 and 1134.1 cm^{-1} (Table 2), which should be multiplied by 0.972 and 0.931 to fit the observed frequencies, respectively. The calculated $^{12}C^{16}O/^{13}C^{16}O$ and $^{12}C^{16}O/^{12}C^{18}O$ isotopic frequency ratios of 1.0237 and 1.0234 (Table 3) are consistent with the experimental values, 1.0239 and 1.0228, respectively. The calculated $^{16}O/^{18}O$ isotopic O−O stretching frequency ratio (1.0607) is also in accord with the experiment (1.0593) (Table 3). Similarly, the good agreement between the experimental and calculated vibrational frequencies, relative absorption intensities, and isotopic shifts confirms the identification of the $(O_2)Cu(CO)_2$ molecule (Tables 2 and 3, Figure 10). Briefly, $(O_2)Cu(CO)_2$ is predicted to have a $^2A_2$ ground state with a C_{2v} symmetry and ∠CCuC of 132.3°, which lies 23.02 kcal/mol lower than the quartet one.

Interestingly, weak CO_2 bands site split at 2344.8, 2339.0 cm^{-1} and 663.5, 661.9 cm^{-1} have been observed after sample deposition, as shown in Figure 1. Annealing to 30 K and $\lambda > 600$ nm irradiation did not enhance these bands. However, the CO_2 bands sharply increased after $\lambda > 340$ nm irradiation and visibly increased upon broad-band irradiation at the expense of the $(O_2)CuCO$ and $(O_2)Cu(CO)_2$ species, suggesting that these carbonyl copper oxides might act as the precursors for the

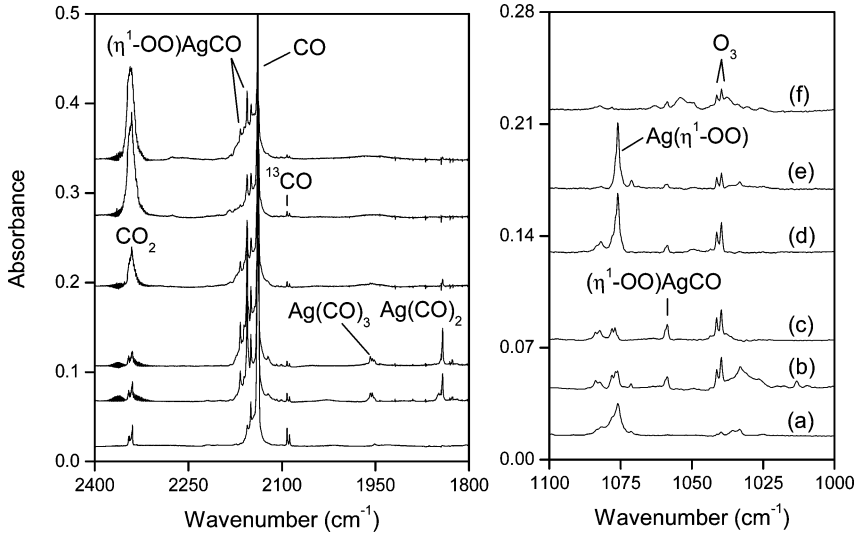

Figure 5. Infrared spectra in the 2400−1800 and 1100−1000 cm^{-1} regions from co-deposition of laser-ablated Ag atoms with 0.25% CO + 0.5% O_2 in Ar: (a) 1 h of sample deposition at 7 K; (b) after annealing to 25 K; (c) after annealing to 30 K; (d) after 20 min of $\lambda > 340$ nm irradiation; (e) after 20 min of broad-band irradiation; (f) after annealing to 34 K.

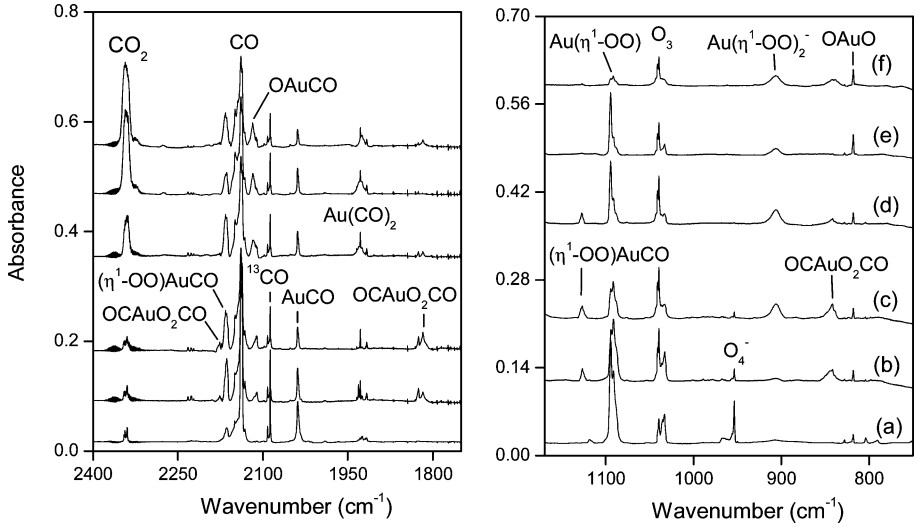

Figure 6. Infrared spectra in the 2400−1800 and 1150−800 cm^{-1} regions from co-deposition of laser-ablated Au atoms with 0.5% CO + 5.0% O_2 in Ar: (a) 1 h of sample deposition at 7 K; (b) after annealing to 25 K; (c) after annealing to 30 K; (d) after 20 min of $\lambda > 340$ nm irradiation; (e) after 20 min of broad-band irradiation; (f) after annealing to 34 K.

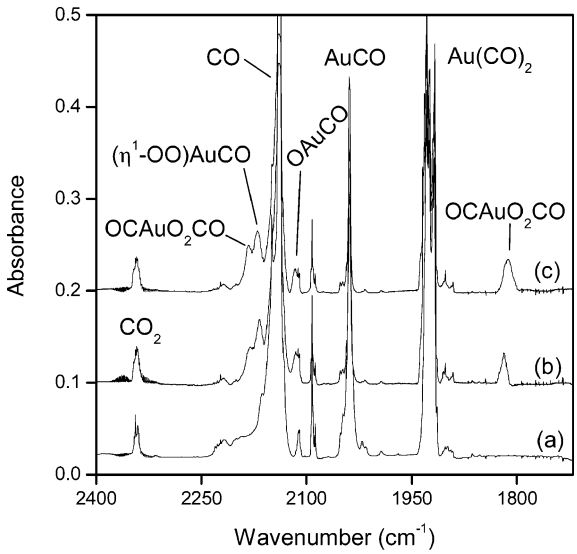

Figure 7. Infrared spectra in the 2400−1800 cm^{-1} region from co-deposition of laser-ablated Au atoms with 5.0% CO + 0.5% O_2 in Ar: (a) 1 h of sample deposition at 7 K; (b) after annealing to 25 K; and (c) after annealing to 30 K.

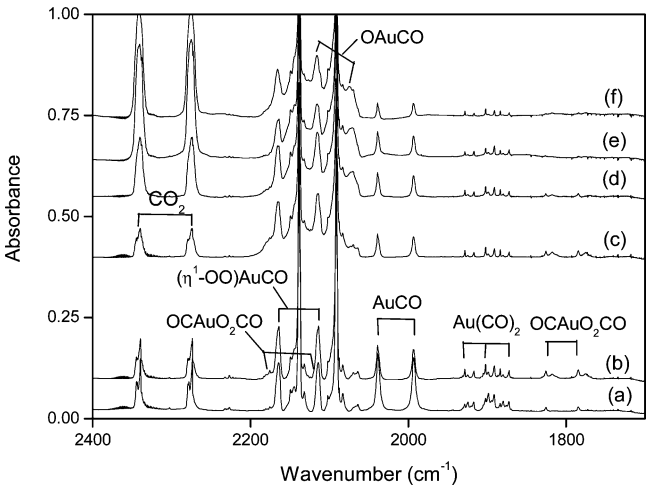

Figure 8. Infrared spectra in the 2400−1800 cm^{-1} region from co-deposition of laser-ablated Au atoms with 0.35% $^{12}C^{16}O$ + 0.35% $^{13}C^{16}O$ + 5.0% O_2 in Ar: (a) 1 h of sample deposition at 7 K; (b) after annealing to 25 K; (c) after annealing to 30 K; (d) after 20 min of $\lambda > 340$ nm irradiation; (e) after 20 min of broad-band irradiation; (f) after annealing to 34 K.

oxidation of CO to CO_2. The $Cu(CO)_n$ ($n = 1-3$) molecules survived during the UV irradiation and annealing.

Ag + CO + O_2. Previous work has shown the formation of $(OC)Ag^+,O_2^-$.[23] In this work, more detailed investigations with complete isotopic substitution have been performed. Figure 5 illustrates infrared spectra for the reaction of laser-ablated Ag atoms with CO/O_2 mixture in excess argon after deposition, ultraviolet photolysis, and annealing. The absorptions at 2166.4, 2155.7, and 1058.7 cm^{-1} have been observed upon sample annealing. These bands decreased together after $\lambda > 340$ nm and broad-band photolysis, and slightly recovered after further annealing. For the C−O stretching mode, the mixed $^{12}C^{16}O$ + $^{13}C^{16}O$ + O_2 and $^{12}C^{16}O$ + $^{12}C^{18}O$ + O_2 isotopic spectra (not shown here) only provide the sum of pure isotopic bands, indicating that only one CO subunit is involved in this mode. The scrambled CO + $^{16}O_2$ + $^{16}O^{18}O$ + $^{18}O_2$ sample gave the oxygen isotopic quartet pattern with 1:1:1:1 intensity profile at 1058.7, 1029.3, 1027.4, and 998.9 cm^{-1}, which suggests that two inequivalent oxygen atoms are involved. Additionally, the CO + $^{16}O_2$ + $^{18}O_2$ experiment only provided the sum of the pure isotopic bands. It can be inferred that the absorption at 2166.4 cm^{-1} belongs to the matrix trapping site of the 2155.7 cm^{-1} band on the basis of the similar growth/decay characteristics as a function of changes of experimental conditions. Accordingly, the 2166.4, 2155.7, and 1058.7 cm^{-1} bands should be assigned to the C−O and O−O stretching modes of (η^1-OO)AgCO in different matrix sites, respectively, which is comparable with the absorptions at 2165 and 1110 cm^{-1} of the previously reported $(OC)Ag^+,O_2^-$.[23]

The present DFT calculations predict that (η^1-OO)AgCO has a $^2A''$ ground state with a C_s symmetry and ∠OAgC of 177.3° (Table 2, Figure 10), which lies 12.30 kcal/mol lower than the quartet one. The calculated $^{12}C^{16}O/^{13}C^{16}O$ and $^{12}C^{16}O/^{12}C^{18}O$ isotopic frequency ratios of 1.0231 and 1.0243 (Table 3) are again in good agreement with the experimental values, 1.0225 and 1.0228, respectively. Also, the calculated $^{16}O/^{18}O$ isotopic O−O stretching frequency ratio (1.0607) is consistent with the experimental value (1.0597) (Table 3). Our DFT calculations lead to the prediction that the oxygen isotopic quartet pattern (i.e., CO + $^{16}O_2$ + $^{16}O^{18}O$ + $^{18}O_2$ spectra) has the approximate

TABLE 1: IR Absorptions (in cm^{-1}) Observed from Co-deposition of Laser-Ablated Cu, Ag, and Au Atoms with CO and O_2 Mixtures in Excess Argon at 7 K

	$CO + O_2$	$^{13}CO + O_2$	$C^{18}O + O_2$	$CO + {}^{18}O_2$	$R(^{12}CO/^{13}CO)$	$R(C^{16}O/C^{18}O)$	$R(^{16}O/^{18}O)$	assignment
Cu	2128.3	2078.6	2080.8	2128.1	1.0239	1.0228	1.0001	$(O_2)CuCO$
	1055.3	1055.3	1055.2	996.2	1.0000	1.0001	1.0593	$(O_2)CuCO$
	2174.7	2126.3	2125.5	2174.6	1.0228	1.0232	1.0000	$(O_2)Cu(CO)_2$
	2114.2	2067.1	2064.8	2114.1	1.0228	1.0239	1.0000	$(O_2)Cu(CO)_2$
	1073.1	1073.1	1073.1	1012.7	1.0000	1.0000	1.0596	$(O_2)Cu(CO)_2$
Ag	2166.4	2118.7	2117.9	2166.4	1.0225	1.0229	1.0000	site
	2155.7	2108.2	2107.6	2155.7	1.0225	1.0228	1.0000	(η^1-OO)AgCO
	1058.7	1058.7	1058.6	998.9	1.0000	1.0001	1.0597	(η^1-OO)AgCO
Au	2166.4	2116.1	2119.2	2165.8	1.0238	1.0223	1.0003	(η^1-OO)AuCO
	1126.8	1124.5	1126.0	1065.7	1.0020	1.0007	1.0573	(η^1-OO)AuCO
	2176.3	2128.0	2127.3	2176.3	1.0227	1.0230	1.0000	$OCAuO_2CO$
	1825.6	1784.5	1786.1	1825.1	1.0230	1.0221	1.0003	$OCAuO_2CO$
	1817.6	1776.6	1778.1	1817.1	1.0231	1.0222	1.0003	site
	842.0	825.4	833.5	829.3	1.0201	1.0102	1.0153	$OCAuO_2CO$
	2118.1	2069.2	2072.6	2118.0	1.0236	1.0220	1.0000	OAuCO

1:1:1:1 intensity profile at 1141.3, 1110.0, 1108.3, and 1076.0 cm^{-1}, which corroborates the (η^1-OO)AgCO assignment.

It can be seen from Figure 5 (traces a−c) that weak bands of CO_2 appeared after sample deposition and almost did not increase upon annealing to 30 K. The IR absorptions of CO_2 observably increased after $\lambda > 340$ nm irradiation and remarkably increased upon broad-band irradiation at the expense of the (η^1-OO)AgCO species and $Ag(CO)_n$ ($n = 2, 3$), exhibiting the oxidation of CO to CO_2 on Ag atom. After further annealing to 34 K, the (η^1-OO)AgCO molecule slightly recovered, while the silver oxides disappeared and the silver carbonyls did not recover.

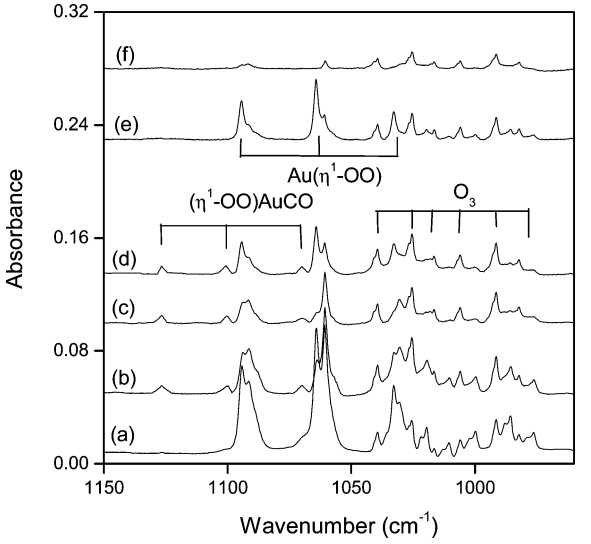

Figure 9. Infrared spectra in the 1150−960 cm^{-1} region from co-deposition of laser-ablated Au atoms with 0.5% CO + 3.5% $^{16}O_2$ + 7.0% $^{16}O^{18}O$ + 3.5% $^{18}O_2$ in Ar: (a) 1 h of sample deposition at 7 K; (b) after annealing to 25 K; (c) after annealing to 30 K; (d) after 20 min of $\lambda > 340$ nm irradiation; (e) after 20 min of broad-band irradiation; (f) after annealing to 34 K.

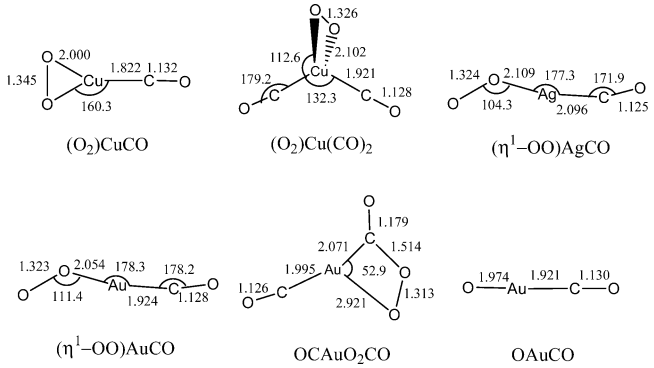

Figure 10. Optimized structures (bond lengths in angstroms and bond angles in degrees) of possible reaction products calculated at the B3LYP/6-311+G(d)-LANL2DZ level.

Au + CO + O_2. Previous work has exhibited the formation of $OCAuO_2CO$ and OAuCO.[24] In this work, we have carried out more detailed experiments with complete isotopic substitution that confirm the formation of $OCAuO_2CO$ and OAuCO and present a new species of (η^1-OO)AuCO.

Figure 6 illustrates infrared spectra for the reaction of laser-ablated Au atoms with CO/O_2 mixture in excess argon after deposition, ultraviolet photolysis, and annealing. New absorptions at 2166.4 and 1126.8 cm^{-1} have been observed after sample deposition. These bands slightly increased upon sample annealing, almost did not change after $\lambda > 340$ nm, observably decreased upon broad-band photolysis, and slightly recovered after further annealing. For the C−O stretching mode, the mixed $^{12}C^{16}O + {}^{13}C^{16}O + O_2$ isotopic spectra (Figure 8) only provide the sum of pure isotopic bands, indicating that only one CO subunit is involved. The $CO + {}^{16}O_2 + {}^{18}O_2$ experiment only provided the sum of the pure isotopic bands (not shown here). However, the scrambled $CO + {}^{16}O_2 + {}^{16}O^{18}O + {}^{18}O_2$ sample (Figure 9) gave the oxygen isotopic triplet pattern with 1:2:1 intensity profile at 1126.8, 1100.6, and 1065.7 cm^{-1}, which suggests that one OO subunit is involved in this molecule. The attachment of OO to Au is uncertain because the intermediate isotopic component (1100.6 cm^{-1}) is near the strong Au(η^1-$^{16}O^{16}O$) absorption and cannot give obvious structural information. Our DFT calculations suggest that (η^1-OO)AuCO has end-on coordination with a bent structure, which is analogous to the (η^1-OO)AgCO complex. Accordingly, the 2166.4 and 1126.8 cm^{-1} bands should be assigned to the C−O and O−O stretching modes of (η^1-OO)AuCO, respectively. Additionally, the absorption of another intermediate isotopic component of (η^1-$^{16}O^{18}O$)-AuCO may be overlapped by the band of Au(η^1-$^{16}O^{16}O$) (Figure 9).

Another group of absorptions at 2176.3 cm^{-1}, 1825.6 cm^{-1} with a matrix trapping site at 1817.6 cm^{-1}, and 842.0 cm^{-1} have also been observed after sample annealing. As shown in Figure 7, these bands sharply increase together with the increase of CO/O_2 ratio. The mixed isotopic pattern (Figure 8) shows that the absorptions at 2176.3, 1825.6, and 842.0 cm^{-1} can be assigned to the C−O stretching vibrations of $OCAuO_2CO$, respectively, consistent with the previous report.[24]

TABLE 2: Ground Electronic States, Point Groups, Vibrational Frequencies (cm^{-1}), and Intensities (km/mol) of Reaction Products Calculated at the B3LYP/6-311+G(d)-LANL2DZ Level

species	electon. state	point group	frequency (intensity, mode)
$(O_2)CuCO$	$^2A_2$	C_{2v}	2190.3 (798, A_1), 1134.1 (105, A_1), 205.9 (5, A_1), 389.2 (2, B_2), 351.1 (36, A_1), 345.7 (0, B_1), 193.1 (5, B_2), 91.8 (10, B_1), 75.5 (3, B_2)
$(O_2)Cu(CO)_2$	$^2A_2$	C_{2v}	2215.0 (326, A_1), 2181.0 (1058, B_2), 1149.5 (202, A_1), 375.1 (11, A_1), 358.6 (17, B_2), 351.1 (4, B_1), 334.0 (0.1, A_1), 317.6 (0, A_2), 303.8 (14, A_1), 272.8 (6, B_2), 195.0 (0, B_1), 104.9 (0, A_2), 62.5 (3, B_1), 44.3 (0.02, A_1), 38.4 (3, B_2)
(η^1-OO)AgCO	$^2A''$	C_s	2220.4 (683, A′), 1141.3 (210, A′), 434.9 (1, A′), 270.4 (1, A′), 255.5 (17, A′), 252.6 (1, A″), 116.2 (28, A′), 54.3 (10, A′), 47.3 (4, A″)
(η^1-OO)AuCO	$^2A''$	C_s	2220.4 (504, A′), 1145.7 (22, A′), 519.5 (7, A′), 421.6 (6, A′), 394.7 (6, A″), 390.7 (5, A′), 187.3 (15, A′), 90.8 (4, A″), 68.9 (3, A′)
$OCAuO_2CO$	$^2A''$	C_s	2232.4 (409, A′), 1881.4 (353, A′), 1182.2 (38, A′), 841.6 (205, A′), 511.1 (38, A′), 506.6 (4, A″), 453.5 (36, A′), 365.9 (2, A′), 341.9 (8, A′), 335.9 (2, A″), 272.4 (3, A′), 141.4 (5, A′), 138.9 (1, A″), 59.6 (1, A″), 53.8 (0.4, A′)
OAuCO	$^2\Pi$	$C_{\infty v}$	2206.3 (603, σ), 547.2 (5, σ), 455.5 (2, π), 429.4 (10, σ), 423.2 (2, π), 109.2 (6, π), 107.7 (8, π)

TABLE 3: Comparison of Observed and Calculated IR Frequency Ratios for the Products

			$R(^{12}CO/^{13}CO)$		$R(C^{16}O/C^{18}O)$		$R(^{16}O/^{18}O)$	
species	freq (cm^{-1})	mode	obsd	calcd	obsd	calcd	obsd	calcd
$(O_2)CuCO$	2128.3	ν_{C-O}	1.0239	1.0237	1.0228	1.0234	1.0001	1.0000
	1055.3	ν_{O-O}	1.0000	1.0000	1.0001	1.0000	1.0593	1.0607
$(O_2)Cu(CO)_2$	2174.7	ν_{C-O}	1.0228	1.0234	1.0232	1.0237	1.0000	1.0000
	2114.2	ν_{C-O}	1.0228	1.0231	1.0239	1.0242	1.0000	1.0000
	1073.1	ν_{O-O}	1.0000	1.0000	1.0000	1.0000	1.0596	1.0606
(η^1-OO)AgCO	2155.7	ν_{C-O}	1.0225	1.0231	1.0228	1.0243	1.0000	1.0000
	1058.7	ν_{O-O}	1.0000	1.0000	1.0001	1.0000	1.0597	1.0607
(η^1-OO)AuCO	2166.4	ν_{C-O}	1.0238	1.0238	1.0223	1.0232	1.0003	1.0000
	1126.8	ν_{O-O}	1.0020	1.0000	1.0007	1.0000	1.0573	1.0607
$OCAuO_2CO$	2176.3	ν_{C-O}	1.0227	1.0234	1.0230	1.0238	1.0000	1.0000
	1825.6	ν_{C-O}	1.0230	1.0235	1.0221	1.0231	1.0003	1.0004
	842.0	ν_{C-O}	1.0201	1.0237	1.0102	1.0102	1.0153	1.0126
OAuCO	2118.1	ν_{C-O}	1.0236	1.0239	1.0220	1.0231	1.0000	1.0000

The 2118.1 cm^{-1} band (Table 1 and Figure 6) is assigned to OAuCO based on the isotopic substitution, whereas a weak, broad band around 2190 cm^{-1} was assigned to this species in the previous work.[24] The OAuCO band appeared after sample annealing; it greatly increased after $\lambda > 340$ nm and broad-band irradiation at the expense of the $OCAuO_2CO$ species.

The present DFT calculations predict that (η^1-OO)AuCO has a $^2A''$ ground state with a C_s symmetry and ∠OAgC of 178.3° (Table 2 and Figure 10), which lies 20.56 kcal/mol lower than the quartet one. The calculated $^{12}C^{16}O/^{13}C^{16}O$ and $^{12}C^{16}O/^{12}C^{18}O$ isotopic frequency ratios of 1.0238 and 1.0232 (Table 3) are in excellent agreement with the experimental values, 1.0238 and 1.0223, respectively. Also, the calculated $^{16}O/^{18}O$ isotopic O−O stretching frequency ratio (1.0607) is in accord with the experiment (1.0573) (Table 3). $OCAuO_2CO$ is predicted to have a $^2A''$ ground state with a C_s symmetry, whereas OAuCO has a $^2\Pi$ ground state with a $C_{\infty v}$ sysmetry (Table 2 and Figure 10). Similar good agreement between the experimental and calculated vibrational frequencies, relative absorption intensities, and isotopic shifts has also been obtained for $OCAuO_2CO$ and OAuCO (Tables 2 and 3).

Similar to copper and silver, co-deposition of laser-ablated Au atoms with CO/O_2 mixture in the present experiments produced weak CO_2 bands (Figure 6). Annealing to 30 K also did not enhance these CO_2 bands. After UV irradiation, the elimination of CO_2 has been observed with the decrease of the (η^1-OO)AuCO and $OCAuO_2CO$ species, whereas the OAuCO species increased and gold carbonyls and oxides survived, indicating that these carbonyl gold oxides may be act as the precursors for the oxidation of CO to CO_2.

Mechanism of CO Oxidation. Under the present experimental conditions, laser-ablated copper, silver, and gold atoms react with CO and O_2 mixture in the excess argon matrixes to produce carbonyl metal oxide species as well as metal carbonyls and metal oxides. In the case of Cu, mainly the $Cu(CO)_n$ (n = 1, 2) molecules are the primary products after sample deposition and survive after photolysis, whereas $Cu(O_2)$ and CuOO slightly appear after sample annealing, slightly increase after further annealing, and disappear on photolysis (Figure 1), indicating that Cu prefers the reaction with CO to the reaction with O_2. For Ag, silver oxides are the primary products after sample deposition and survive after photolysis, whereas silver carbonyls slightly appear after sample annealing, slightly increase after further annealing, and disappear on photolysis (Figure 5), implying that Ag prefers the reaction with O_2 to the reaction with CO. For Au, gold carbonyls and oxides appeared together after sample deposition and (η^1-OO)AuCO and $OCAuO_2CO$ increased at the expense of these gold carbonyls and oxides (Figure 6), indicating that the reactivity of Au to CO is comparable to that of O_2. As shown in Figures 1, 5, and 6, traces of CO_2 appeared after sample deposition and almost did not increase upon annealing, indicating that they may be produced by radiation from the ablation plume. After UV irradiation, CO_2 greatly increased at the expense of carbonyl metal oxides; furthermore, silver carbonyls disappeared, but copper and gold higher carbonyls increased, showing the oxidation of CO to CO_2 on Cu, Ag, and Au atoms. It is noted that in all the cases only the isotopic form $C^{16}O^{18}O$ has been observed in the CO + $^{18}O_2$ experiment, implying that one oxygen atom in the CO_2 production is from CO and another one is from O_2.

SCHEME 1: Reaction Pathways of Laser-Ablated Cu, Ag, and Au Atoms with CO/O_2 Mixtures in Solid Argon

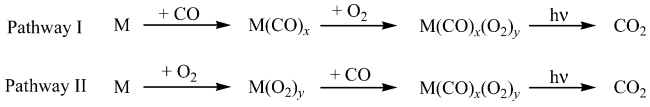

Scheme 1 presents the possible reaction pathways for laser-ablated group 11 metal atoms with CO and O_2 mixture in argon

matrixes. The reactivity toward CO and O_2 is found to be considerably different for Cu, Ag, and Au. Based on the above-mentioned findings, it could be inferred that the reactivity of copper toward CO is prior to O_2, the reactivity of silver toward O_2 is prior to CO, and the reactivity of gold toward CO is comparable to O_2. In the reaction of Cu, Ag, and Au atoms with CO/O_2 mixture, Cu prefers pathway I and Ag prefers pathway II, while pathways I and II are parallel for Au. On the other hand, the effect of UV irradiation on $M(O_2)$ complexes has been shown previously to induce insertion and formation of metal oxide OMO.[19] In the present experiments, copper carbonyls, silver oxides, and gold carbonyls and oxides remain after photolysis. Upon UV irradiation, it is possible that the inserted OMO directly reacts with CO to produce CO_2, and this reaction may also contribute to some extent to the CO_2 production.

The metal $(n - 1)d_\pi$, *n*s, *n*p, and CO $2\pi^*$ energy levels may be helpful to understand this difference in the reactivity of group 11 metal atoms toward CO and O_2. Taking the Cu−CO pair as an example, the Cu $3d_\pi$ and CO π^* levels are close (ca. 73.37 kcal/mol), but the Cu 4s and CO lone-pair levels are far apart (ca. 96.85 kcal/mol),[11d] and thus the $d_\pi \rightarrow \pi^*$ back-donation is primarily responsible for the thermal stability of CuCO, consistent with previous reports.[18c] As previously reported,[18c] the absence of AgCO complex is attributed to the larger gap between Ag 4d and CO π^* levels relative to Cu. For the Au−CO pair, the metal d_π and CO π^* levels are further apart than those in the Cu−CO case, but the metal s and the CO lone-pair levels are closer. It has been found that the contribution of the formation of AuCO is mainly from a larger σ-type dative interaction. That is, the formation of AuCO is easier than that of AgCO, but more difficult than that of CuCO. Consequently, the reaction pathways of gold toward CO and O_2 are comparable when Au faces simultaneously the CO and O_2 molecules; silver forms silver oxides prior to the silver carbonyls, whereas copper prefers the formation of copper carbonyls to that of copper oxides.

Conclusions

Reactions of laser-ablated Cu, Ag, and Au atoms with CO and O_2 mixture in solid argon have been studied using matrix-isolation infrared spectroscopy. Besides the metal carbonyls and oxides, the carbonyl metal oxides, $(O_2)Cu(CO)_n$ ($n = 1, 2$), (η^1-OO)MCO (M = Ag, Au), $OCAuO_2CO$, and OAuCO, are formed on sample deposition or annealing and are characterized using infrared spectroscopy on the basis of the results of the isotopic substitution and the CO concentration change. UV irradiation on these carbonyl metal oxides produced CO_2, indicating the oxidation of carbon monoxide to carbon dioxide. The present experiments show that the reactivity of copper toward CO is prior to O_2, the reactivity of silver toward O_2 is prior to CO, and the reactivity of gold toward CO is comparable to O_2. Density functional theory (DFT) calculations have been performed on these molecules. The identifications of these carbonyl metal oxides are confirmed by the good agreement between the experimental and calculated vibrational frequencies, relative absorption intensities, and isotopic shifts.

Acknowledgment. We thank the reviewer for valuable suggestions. This work was supported by a Grant-in-Aid for Scientific Research (B) (Grant 17350012) from the Ministry of Education, Culture, Sports, Science and Technology (MEXT) of Japan and by Marubun Research Promotion Foundation. L.J. thanks the MEXT of Japan and Kobe University for an Honors Scholarship.

References and Notes

(1) Haruta, M. *Catal. Today* **1997**, *36*, 153.

(2) See, for example: Haruta, M.; Yamada, N.; Kobayashi, T.; Iijima, S. *J. Catal.* **1989**, *115*, 301. Haruta, M.; Tsubota, S.; Kobayashi, T.; Kageyama, H.; Genet, M. J.; Delmon, B. *J. Catal.* **1993**, *144*, 175. Haruta, M. *Stud. Surf. Sci. Catal.* **2001**, *145*, 31. Sanchez-Castillo, M. A.; Couto, C.; Kim, W. B.; Dumesic, J. A. *Angew. Chem., Int. Ed. Engl.* **1983**, *43*, 1140. Bond, G. C.; Thompson, D. T. *Catal. Rev.*—Sci. Eng. **1999**, *41*, 319. Molina, L. M.; Hammer, B. *J. Catal.* **2005**, *233*, 399.

(3) Sanchez, A.; Abbet, S.; Heiz, U.; Schneider, W. D.; Hakkinen, H.; Barnett, R. N.; Landman, U. *J. Phys. Chem. A* **1999**, *103*, 9573.

(4) Stolcic, D.; Fischer, M.; Ganteför, G.; Kim, Y. D.; Sun, Q.; Jena, P. *J. Am. Chem. Soc.* **2003**, *125*, 2848. Kimble, M. L.; Castleman, A. W., Jr.; Mitric, R.; Burgel, C.; Bonacic- Koutecky, V. *J. Am. Chem. Soc.* **2004**, *126*, 2526.

(5) Wallace, W. T.; Whetten, R. L. *J. Am. Chem. Soc.* **2002**, *124*, 7499.

(6) Hagen, J.; Socaciu, L. D.; Elijazyfer, M.; Heiz, U.; Bernhardt, T. M.; Woste, L. *Phys. Chem. Chem. Phys.* **2002**, *4*, 1707. Socaciu, L. D.; Hagen, J.; Bernhardt, T. M.; Woste, L.; Heiz, U.; Hakkinen, H.; Landman, U. *J. Am. Chem. Soc.* **2003**, *125*, 10437.

(7) Zhai, H. J.; Kiran, B.; Dai, B.; Li, J.; Wang, L. S. *J. Am. Chem. Soc.* **2005**, *127*, 12098.

(8) van Herwijnen, T.; de Jong, W. A. *J. Catal.* **1980**, *63*, 83. Campbell, C. T.; Daube, K. A. *J. Catal.* **1980**, *104*, 109. Nakumura, J.; Campbell, J. M.; Campbell, C. T. *J. Chem. Soc., Faraday Trans.* **1990**, *86*, 2725. Wang, G. C.; Jiang, L.; Cai, Z. S.; Pan, Y. M.; Zhao, X. Z.; Huang, W.; Xie, K. C.; Li, Y. W.; Sun, Y. H.; Zhong, B. *J. Phys. Chem. B* **2003**, *107*, 557.

(9) Chinchen, G. C.; Spencer, M. S.; Waugh, K. C.; Whan, D. A. *J. Chem. Soc., Faraday Trans.1* **1987**, *83*, 2193. Jiang, L.; Wang, G. C.; Cai, Z. S.; Pan, Y. M.; Zhao, X. Z. *J. Mol. Struct. (Theochem)* **2004**, *710*, 97.

(10) See, for example: Xu, C.; Manceron, L.; Perchard, J. P. *J. Chem. Soc., Faraday Trans.* **1993**, *89*, 1291. Bondybey, V. E.; Smith, A. M.; Agreiter, J. *Chem. Rev.* **1996**, *96*, 2113. Fedrigo, S.; Haslett, T. L.; Moskovits, M. *J. Am. Chem. Soc.* **1996**, *118*, 5083. Khriachtchev, L.; Pettersson, M.; Runeberg, N.; Lundell, J.; Rasanen, M. *Nature* **2000**, *406*, 874. Himmel, H. J.; Manceron, L.; Downs, A. J.; Pullumbi, P. *J. Am. Chem. Soc.* **2002**, *124*, 4448. Li, J.; Bursten, B. E.; Liang, B.; Andrews, L. *Science* **2002**, *295*, 2242. Andrews, L.; Wang, X. *Science* **2003**, *299*, 2049.

(11) (a) Zhou, M. F.; Tsumori, N.; Li, Z.; Fan, K.; Andrews, L.; Xu, Q. *J. Am. Chem. Soc.* **2002**, *124*, 12936. (b) Zhou, M. F.; Xu, Q.; Wang, Z.; von Ragué Schleyer, P. *J. Am. Chem. Soc.* **2002**, *124*, 14854. (c) Jiang, L.; Xu, Q. *J. Am. Chem. Soc.* **2005**, *127*, 42. (d) Jiang, L.; Xu, Q. *J. Am. Chem. Soc.* **2005**, *127*, 8906. (e) Xu, Q.; Jiang, L.; Tsumori, N. *Angew. Chem., Int. Ed.* **2005**, *44*, 4338.

(12) Burkholder, T. R.; Andrews, L. *J. Chem. Phys.* **1991**, *95*, 8697. Zhou, M. F.; Tsumori, N.; Andrews, L.; Xu, Q. *J. Phys. Chem. A* **2003**, *107*, 2458. Jiang, L.; Xu, Q. *J. Chem. Phys.* **2005**, *122*, 034505.

(13) Frisch, M. J.; Trucks, G. W.; Schlegel, H. B.; Scuseria, G. E.; Robb, M. A.; Cheeseman, J. R.; Montgomery, J. A., Jr.; Vreven, T.; Kudin, K. N.; Burant, J. C.; Millam, J. M.; Iyengar, S. S.; Tomasi, J.; Barone, V.; Mennucci, B.; Cossi, M.; Scalmani, G.; Rega, N.; Petersson, G. A.; Nakatsuji, H.; Hada, M.; Ehara, M.; Toyota, K.; Fukuda, R.; Hasegawa, J.; Ishida, M.; Nakajima, T.; Honda, Y.; Kitao, O.; Nakai, H.; Klene, M.; Li, X.; Knox, J. E.; Hratchian, H. P.; Cross, J. B.; Adamo, C.; Jaramillo, J.; Gomperts, R.; Stratmann, R. E.; Yazyev, O.; Austin, A. J.; Cammi, R.; Pomelli, C.; Ochterski, J. W.; Ayala, P. Y.; Morokuma, K.; Voth, G. A.; Salvador, P.; Dannenberg, J. J.; Zakrzewski, V. G.; Dapprich, S.; Daniels, A. D.; Strain, M. C.; Farkas, O.; Malick, D. K.; Rabuck, A. D.; Raghavachari, K.; Foresman, J. B.; Ortiz, J. V.; Cui, Q.; Baboul, A. G.; Clifford, S.; Cioslowski, J.; Stefanov, B. B.; Liu, G.; Liashenko, A.; Piskorz, P.; Komaromi, I.; Martin, R. L.; Fox, D. J.; Keith, T.; Al-Laham, M. A.; Peng, C. Y.; Nanayakkara, A.; Challacombe, M.; Gill, P. M. W.; Johnson, B.; Chen, W.; Wong, M. W.; Gonzalez, C.; Pople, J. A. *Gaussian 03*, revision B.04; Gaussian, Inc.: Pittsburgh, PA, 2003.

(14) Becke, A. D. *Phys. Rev. A* **1988**, *38*, 3098. Perdew, J. P. *Phys. Rev. B* **1986**, *33*, 8822. Lee, C.; Yang, E.; Parr, R. G. *Phys. Rev. B* **1988**, *37*, 785. Becke, A. D. *J. Chem. Phys.* **1993**, *98*, 5648.

(15) McLean, A. D.; Chandler, G. S. *J. Chem. Phys.* **1980**, *72*, 5639. Krishnan, R.; Binkley, J. S.; Seeger, R.; Pople, J. A. *J. Chem. Phys.* **1980**, *72*, 650. Frisch, M. J.; Pople, J. A.; Binkley, J. S. *J. Chem. Phys.* **1984**, *80*, 3265.

(16) Hay, P. J.; Wadt, W. R. *J. Chem. Phys.* **1985**, *82*, 299.

(17) Huber, H.; Kundig, E. P.; Moskovits, M.; Ozin, G. A. *J. Am. Chem. Soc.* **1975**, *97*, 2097. Kasai, P. H.; Jones, P. M. *J. Am. Chem. Soc.* **1985**, *107*, 813. Chenier, J. H. B.; Hampson, C. A.; Howard, J. A.; Mile, B. *J. Phys. Chem.* **1989**, *93*, 114. Blitz, M. A.; Mitchell, S. A.; Hackett, P. A. *J. Phys. Chem.* **1991**, *95*, 8719. Zhou, M. F.; Andrews, L. *J. Chem. Phys.* **1999**, *111*, 4548.

(18) (a) McIntosh, D.; Ozin, G. A. *J. Am. Chem. Soc.* **1976**, *98*, 3167. (b) Kasai, P. H.; Jones, P. M. *J. Phys. Chem.* **1985**, *89*, 1147. (c) Kasai, P.

H.; Jones, P. M. *J. Am. Chem. Soc.* **1985**, *107*, 6385. (d) Marian, C. M. *Chem. Phys. Lett.* **1993**, *215*, 582. (e) Liang, B.; Andrews, L. *J. Phys. Chem. A* **2000**, *104*, 9156. (f) Jiang, L.; Xu, Q. *J. Phys. Chem. A* **2005**, *109*, 1026.

(19) Tevault, D. E. *J. Chem. Phys.* **1982**, *76*, 2859. Ozin, G. A.; Mitchell, S. A.; Garcia-Prieto, J. *J. Am. Chem. Soc.* **1983**, *105*, 6399; *J. Phys. Chem.* **1982**, *86*, 473. McIntosh, D.; Ozin, G. A. *Inorg. Chem.* **1976**, *15*, 2869; *Inorg. Chem.* **1977**, *16*, 59. Chertihin, G. V.; Andrews, L.; Bauschlicher, C. W., Jr. *J. Phys. Chem. A* **1997**, *101*, 4026. Wang, X. F.; Andrews, L. *J. Phys. Chem. A* **2001**, *105*, 5812. Citra, A.; Andrews, L. *J. Mol. Struct. (Theochem)* **1999**, *189*, 95.

(20) Thompson, W. E.; Jacox, M. E. *J. Chem. Phys.* **1989**, *91*, 3826. Zhou, M. F.; Hacaloglu, J.; Andrews, L. *J. Chem. Phys.* **1999**, *110*, 9450. Chertihin, G. V.; Andrews, L. *J. Chem. Phys.* **1998**, *108*, 6404.

(21) Zhou, M. F.; Andrews, L.; Bauschlicher, C. W., Jr. *Chem. Rev.* **2001**, *101*, 1931.

(22) (a) Mascetti, J.; Tranquille, M. *J. Phys. Chem.* **1988**, *92*, 2177. (b) Zhou, M. F.; Liang, B. Y.; Andrews, L. *J. Phys. Chem. A* **1999**, *103*, 2013.

(23) Huber, H.; Ozin, G. A. *Inorg. Chem.* **1977**, *16*, 64.

(24) Huber, H.; McIntosh, D.; Ozin, G. A. *Inorg. Chem.* **1977**, *16*, 975.